Impact of the anion on electrochemically doped regionegular and regionandom poly(3-hexylthiophene)

Kyle N. Baustert, ¹ Ashkan Abtahi, ^{1,2,3} Ahmed Ayyash, ¹ Kenneth R. Graham^{1,*}

¹·K. N. Baustert, Dr. A. Abtahi, A. Ayyash, Prof. K. R. Graham Department of Chemistry, University of Kentucky, Lexington, Kentucky, USA E-mail: kenneth.graham@uky.edu

²Department of Physics and Astronomy, University of Kentucky, Lexington, Kentucky, USA

³Department of Chemistry, Purdue University, West Lafayette, Indiana, USA

Keywords: electrochemical doping, conjugated polymers, spectroelectrochemistry, polaron, counterion

Abstract

Chemical and electrochemical doping of π -conjugated polymers is an important aspect in determining the performance and enabling the operation of many organic electronic devices, from organic light emitting diodes and thermoelectrics to organic electrochemical transistors. In both chemical doping and electrochemical doping an ionized dopant or counterion is present along with the doped π -conjugated polymer. This dopant or counterion is not a benign spectator, rather, its presence can significantly impact the optical, electronic, and thermoelectric properties of the resulting material. Here, we investigate how counterion structure impacts the electrochemical doping ability, oxidation potential, ionization energy, and polaron absorbance of regioregular (rr) and regiorandom (rra) P3HT. We find that in most cases the anion has a small effect on the polymer oxidation potential, except for in the case of rr-P3HT with the large tetrakis[3,5-bis(trifluoromethyl)phenyl]borate anion. We propose that this large anion is excluded from the crystalline regions and thus the oxidation potential is similar to that of rra-P3HT. The anions also result in significant differences in polaron absorbance and ionization energies, thereby emphasizing the important role of the

counterion in determining the optical and electronic properties of doped π -conjugated polymers.

1. Introduction

Organic semiconductors (OSC) are currently being used and investigated for multiple applications, many of which involve chemical or electrochemical doping to introduce charge carriers. 1,2 For example, chemical doping is used to improve the performance metrics of organic light emitting diodes and organic photovoltaic cells, ³⁻⁶ respectively, while electrochemical doping or de-doping is used to change the electrical conductivity of organic electrochemical transistors (OECTs).^{7,8} The primary purpose of the dopant in chemical doping is to introduce a charge carrier, while in electrochemical doping the role of the counterion is to balance the overall charge in a material upon charge carrier injection or extraction. However, the impact of the chemical dopant or counterion is not that simple. The addition of the dopant or counterion can significantly impact the OSC morphology and interact differently with the polaron on the OSC depending on the structure of the dopant or counterion. 9-12 In fact, the nature of the chemical dopant or counterion can significantly impact the optical, ¹³ electronic, ^{13–16} and thermoelectric properties of the doped OSC. ^{12,17} An improved understanding of dopant or counterion effects on both the crystalline and amorphous phases of π -conjugated polymers (CPs) is becoming exceedingly important for their continued development. 18,19

Organic semiconductors typically require doping to increase the number of charge carriers and electrical conductivity.²⁰ Additionally, introducing low amounts of a dopant can increase the charge-carrier mobility in the OSC.²¹ There are two primary doping methods, including chemical doping, which can occur through a number of different mechanisms (e.g., acid doping,²² oxidative doping,^{15,23} hydride transfer,^{24,25} etc.) and electrochemical

doping.^{17,26,27} Chemical doping requires matching the energetics of the dopant with the OSC and it is often difficult to control the extent of doping.²⁸ Alternatively, electrochemical doping works by oxidizing or reducing the OSC through applying a potential to a conductive electrode in an electrochemical cell and balances the charge with the influx of anions (or cations) into the material. Electrochemical doping thereby allows more control over the charge-carrier density by varying the applied potential while monitoring the current.

Additionally, it enables the coupling of measurements such as UV-Vis-NIR absorbance spectroscopy with electrochemistry to probe real time changes in absorbance at well-controlled doping levels. Furthermore, electrochemical doping is much less likely to result in the formation of charge-transfer complexes.¹⁵

One class of devices that rely on electrochemical doping are organic electrochemical transistors (OECTs),⁸ which are garnering increasingly more attention due to their growing interest for sensing and bioelectronic applications.²⁹ These OECTs operate based on electrochemical control of the doping level, where small changes in the gate-source bias can result in large changes in the electrical conductivity owing to the electrochemical doping or de-doping processes taking place.³⁰ Several studies have demonstrated that the doping behavior can be highly dependent on the electrolyte ions.^{9,14} For example, the Ginger group showed that different anions require up to 0.2 V differences in gate-source bias to dope P3HT to similar levels,⁹ while work from the Rivnay group showed that larger anions lead to higher threshold voltages and effective capacitance with poly(2-(3,3'-bis(2-(2-(2-methoxyethoxy)-thoxy)-[2,2'-bithiophen]-5-yl)thieno[3,2-b] thiophene) [p(g2T-TT)].¹⁴

Another reason that it is important to investigate the impact of the counterion structure on electrochemical doping behavior is that electrochemistry is often used to extract HOMO and LUMO energies of OSCs.^{31–33} In these measurements the nature of the electrolyte is typically ignored. In addition, voltammetry measurements are sometimes recorded with the OSC dissolved in solution, which neglects the large influence of intermolecular interactions

and morphology on OSC energetics.^{34–37} To enable better interpretation of electrochemically extracted HOMO and LUMO energies it is critical to understand how the electrolyte will affect the oxidation and reduction behavior. Although poly(3-hexylthiophene-2,5-diyl) (P3HT) is one of the more commonly studied CPs, there is still a broad range of reported HOMO and LUMO energies as measured with cyclic voltammetry (CV), with the LUMO energies ranging from -3.53 to -2.70 eV and the HOMO energies spanning a more narrow range from -4.92 to -5.20 eV vs. vacuum.^{38,39,40} These variations in measured energies could be the result of many different factors, including CP film preparation, choice of electrolyte, and solvent system.³⁹

Here, we investigate how counterion structure impacts the electrochemical doping ability, oxidation potential, polaron absorbance, and ionization energy of regioregular (rr) and regiorandom (rra) P3HT. The comparison between rr-P3HT and rra-P3HT provides a platform for comparing doping in crystalline and amorphous regions, with rr-P3HT containing both crystalline and amorphous regions while rra-P3HT is amorphous. To probe how anion size and extent of fluorination impact electrochemical doping, a series of borate anions functionalized with substituents of varying size and number of fluorine atoms are selected. We find that in most cases the anion has a small effect on the polymer oxidation potential, except for in the case of rr-P3HT with B(Ph(CF₃)₂)₄ as a counterion. We propose that B(Ph(CF₃)₂)₄ is excluded from the crystalline regions and as a result the oxidation potential is similar to that of rra-P3HT. Although the large B(Ph(CF₃)₂)₄ anion is excluded from the crystalline regions, the distinct transitions evident in the high-energy polaron band suggest that polarons are primarily formed in the crystalline regions and are spatially separated from the anion. Decreasing the Coulomb interaction through spatially separating the polaron and counterion could provide a powerful means of increasing charge-carrier mobility and electrical conductivity in CPs.

2. Results and Discussion

The structures of the polymers and dopants investigated are depicted in **Figure 1**. All anions discussed are based on tetrasubstituted borates, thereby ensuring similar anion shapes with drastically different sizes. Here, the anion molar volume increases nearly 8 fold from 53.4 cm³mol⁻¹ for BF₄⁻ to 415 cm³mol⁻¹ for B(Ph(CF₃)₂)₄⁻.⁴¹.⁴² The family of tetraphenyl borates contain varying extents of fluorination, with the original intent of varying the electronegativity of the periphery. Tetraphenylborate was also investigated; however, the spectroelectrochemistry data presented in SI Figure S1 and S2 show that tetraphenylborate is unable to support significant polaron formation on rr-P3HT or rra-P3HT. This inability to significantly oxidize the P3HT derivatives with tetraphenylborate as the anion in the electrolyte likely arises from the oxidation of tetraphenylborate prior to oxidation of the P3HT derivatives. On the other hand, the fluorine functionalized tetraphenylborate derivatives are more effective in stabilizing the oxidized P3HT owing to the electron withdrawing fluorine atoms.

Electrochemical doping of conjugated polymers relies in part on the ability of the electrolyte solution to slightly swell the polymer film, ^{27,43} which permits counterion penetration to stabilize the electrochemically doped polymer. If the anions in the electrolyte are unable to penetrate into the polymer film, there will be no balance of this positive charge and primarily surface oxidation will occur. ⁴⁴ It is therefore important to consider ion penetration and solvent penetration in interpreting CV spectra of CP films.

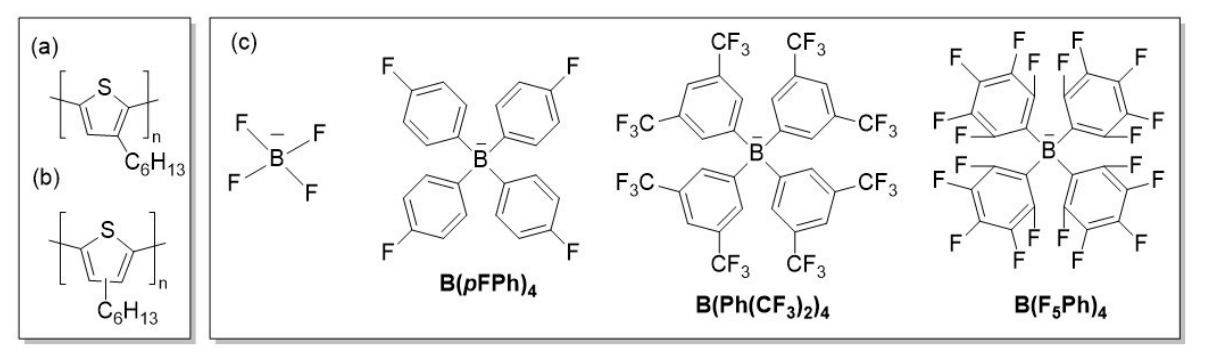


Figure 1. Structures of rr-P3HT (a), rra-P3HT (b), and anions (c).

The cyclic voltammograms displayed in Figure 2a and b show distinct differences based both on the polymer and the anion in the electrolyte. When looking at the comparison of the electrolytes used with rr-P3HT, there are clear differences both in the shapes of the voltammograms as well as the positions of their respective first oxidation peaks, as shown in **Table 1.** Comparing the largest anion, B(Ph(CF₃)₂)₄, to the smallest anion, BF₄, a significant shift of 0.25 V in the first oxidation peak is observed. Scan rate dependent measurements, as presented in SI Figure S3 and S4, show similar trends in the CV spectra with the varying anions for scan rates from 1 to 100 mV/s. Here, even at low scan rates of 1 and 5 mV/s, oxidation of rr-P3HT with B(Ph(CF₃)₂)₄ requires higher potentials than for BF₄ and $B(pFPh)_4$. These similar trends in the voltammograms indicate that the shift in oxidation potential is not a purely kinetic phenomenon. Additionally, the oxidation onset is more gradual with B(Ph(CF₃)₂)₄ as compared to BF₄. Further insight into the reasons for the increase in oxidation potential can be gained through comparison to rra-P3HT, as shown in Figure 2b and c, which shows a more minimal shift of only 0.08 eV between B(Ph(CF₃)₂)₄ and BF₄. The oxidation peak position is also nearly identical for both rr- and rra-P3HT with B(Ph(CF₃)₂)₄ as the anion. We hypothesize that the shift in the oxidation peak position in rr-P3HT is the result of the inability of the large B(Ph(CF₃)₂)₄ anion to penetrate into the crystalline regions. Thus, the low energy oxidation of the crystalline phase of rr-P3HT is nearly absent. Previous work has demonstrated ion uptake is suppressed in stiffer and more ordered regions of P3HT films, 45 and it would follow that ion uptake in these more ordered regions will be further suppressed as the counterion size increases. However, a clear and generalizable picture is yet to be established, as large dodecaboranes have been shown to penetrate into the crystalline regions of rr-P3HT films.¹³

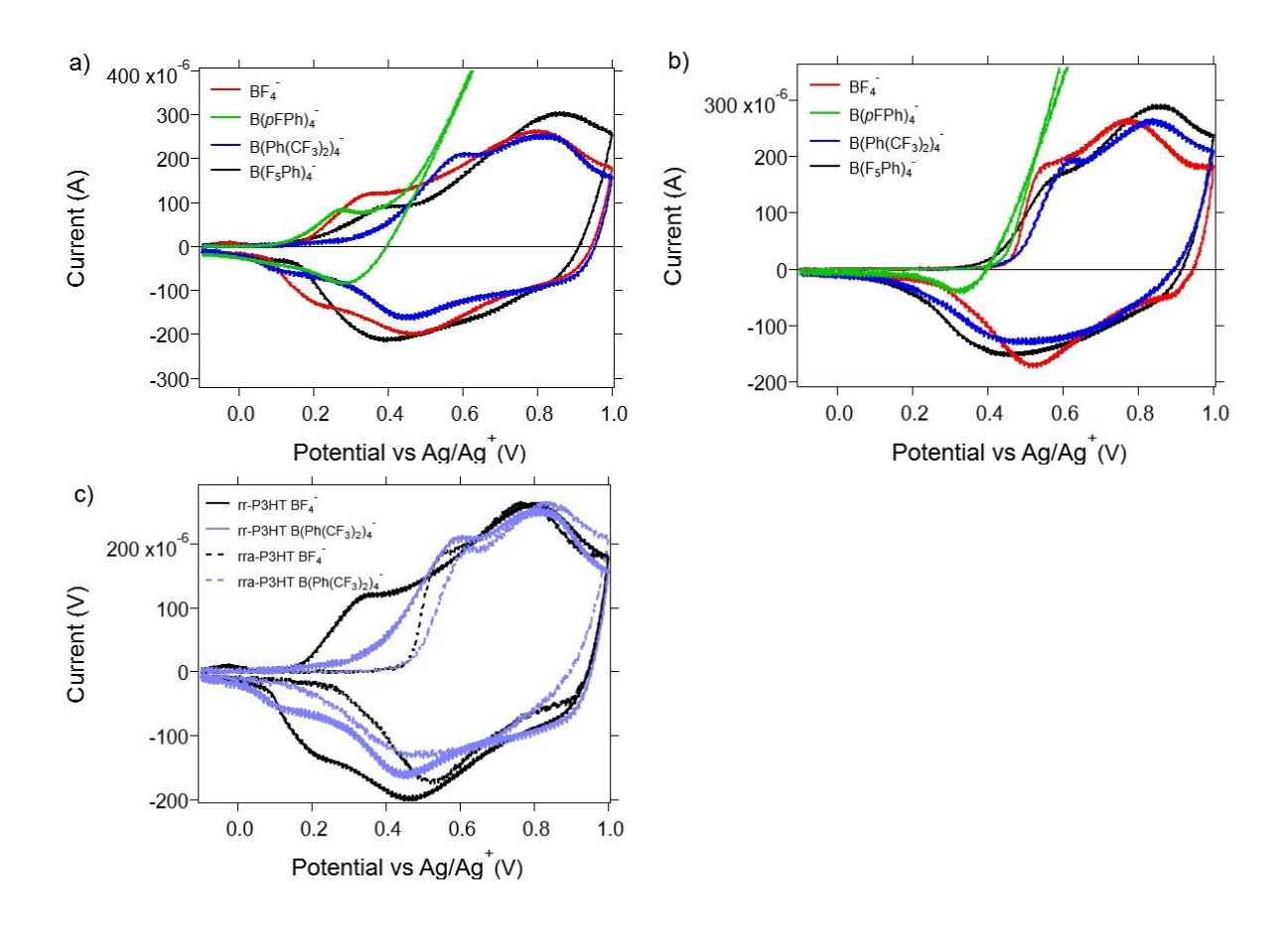


Figure 2. Cyclic voltammograms of rr-P3HT (a) and rra-P3HT (b) with different anions in acetonitrile. Comparison of CVs for rr-P3HT and rra-P3HT using the anions BF_4^- and $B(Ph(CF)_3)_2)_4^-$ (c) in the electrolyte. All CVs were measured from -0.1 V to 1.0 V and back at 20 mV/s.

Table 1. First oxidation peak potentials from CV for rr-P3HT and rra-P3HT with varying anions.

	BF ₄ -(V)	B(<i>p</i> FPh) ₄ - (V)	B(Ph(CF ₃) ₂) ₄ - (V)	B(F ₅ Ph) ₄ - (V)
rr-P3HT	0.34	0.27	0.59	0.38
rra-P3HT	0.54	NAª	0.62	0.57

a) The rra-P3HT oxidation peak cannot be identified due to overlap with B(pFPh)₄ oxidation.

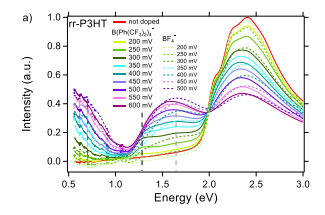
The voltammograms for $B(pFPh)_4^-$ with both rra- and rr-P3HT are very different from the other anions and show a large spike in current beginning near 0.5 V and less reversibility. We attribute this higher current and decreased reversibility to oxidation of $B(pFPh)_4^-$ itself. Supporting Information **Figure S5** offers further support for $B(pFPh)_4^-$ oxidation, which

begins at ca. 0.5 V. Unfortunately, the oxidation of $B(pFPh)_4^-$ and $B(Ph)_4^-$ at relatively low potentials excludes using this family of anions to probe the influence of the electronegativity of the anion periphery.

With the potential impact of ion penetration into crystalline vs. amorphous regions, we turn to rra-P3HT for a more simplified analysis of how the anion impacts the oxidation potential. The anion BF4 displays the steepest oxidation onset and the smallest separation between the first oxidation peak and the associated reduction peak. This trend suggests that BF4 is able to rapidly penetrate into and out-of rra-P3HT, whereas the larger anions are more kinetically limited. Although the oxidation peak with B(F5Ph)4 occurs at a slightly higher potential than with BF4, if the tangent method is used to define the oxidation onset and calculate the HOMO level then using B(F5Ph)4 as the anion leads to a lower (less negative) calculated HOMO level. Furthermore, at low scan speeds of 1 and 5 mV/s the oxidation peak of rra-P3HT with B(F5Ph)4 occurs at a lower potential than for BF4, as shown in SI Figure S4. These measurements further highlight how electrolyte choice can impact the extracted HOMO values, with the subtle shifts likely originating from differing interactions between the different anions and rra-P3HT.

UV-Vis-NIR absorbance spectra for both rr- and rra-P3HT with a series of counterions were recorded as a function of applied potential during a linear staircase voltammetry measurement (**Figure 3**, S1, and S2). The UV-Vis-NIR absorbance spectra for both polymers show clear signs of electrochemical doping, as evident through a reduction in the neutral peak intensities around 2.45 eV for rr-P3HT and 2.75 eV for rra-P3HT and corresponding increases in the polaron absorbance appearing at energies below 2 eV. Looking at the higher energy polaron bands that spans between 1.2 and 1.9 eV there are two different transitions evident for rr-P3HT and predominantly one for rra-P3HT. In rr-P3HT the lower energy transition occurs at *ca.* 1.3 eV and is readily observed for the 300 mV spectra with B(Ph(CF₃)₂)₄- as the counter

anion. The second transition occurs at approximately 1.65 eV, as indicated with the dashed gray line. The 1.3 eV transition is more prevalent at lower applied potentials for $B(Ph(CF_3)_2)_4$ and appears only weakly in the 250 and 300 mV spectra with BF_4 . We suspect that this 1.3 eV transition arises from polarons that are created in the crystalline phase while the counter anions are spatially separated and remain in the amorphous phase. The 1.65 eV transition assignment to polarons in the amorphous phase is supported based on comparison to rra-P3HT. In rra-P3HT the only high energy polaron peak falls \sim 1.60 eV and there is a shift of approximately 60 meV in the peak position between BF_4 and $B(Ph(CF_3)_2)_4$ as anions. The slight differences in both peak position and shape further highlight the importance of the anion in influencing the nature of the polarons, even in amorphous CPs.



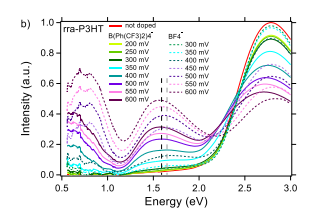
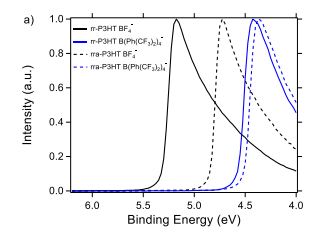


Figure 3. Comparison of spectroelectrochemistry data for rr-P3HT (a) and rra-P3HT (b) with BF_4^- (dashed lines) and $B(Ph(CF)_3)_2)_4^-$ (solid lines) as anions in the electrolyte. Vertical dashed lines highlight the polaron absorption peaks with $B(Ph(CF)_3)_2)_4^-$ (black and gray for rr-P3HT and black only for rra-P3HT) and BF_4^- (gray).

UPS spectra were obtained on electrochemically doped CP films that were doped to their respective first oxidation peaks. Such doping was carried out by increasing the voltage bias at a rate of 20 mV/s and removing the film from solution while it was at the first oxidation peak potential. The films were then rinsed with acetonitrile to remove excess electrolyte on the surface and dried with a nitrogen flow before transferring to the ultra high vacuum system. The UPS data presented in **Figure 4a** and **b** correlate with the previously

discussed CV results in that there is a much more drastic change in the ionization energies (IEs) for rr-P3HT based on the anion than there is for rra-P3HT. In all materials the occupied states extend to the Fermi energy, as is typical for heavily *p*-doped CPs.⁴⁶ However, the work function increases from 4.88 eV for rr-P3HT with BF₄⁻ to 5.60 eV with B(Ph(CF₃)₂)₄⁻. In parallel with the CV results, the IEs for rr- and rra-P3HT with B(Ph(CF₃)₂)₄⁻ are similar at 5.55 and 5.60 eV, respectively, yet the IEs differ by 0.50 eV for rr- and rra-P3HT when BF₄⁻ serves as the counterion. These measurements offer additional support to the hypothesis that B(Ph(CF₃)₂)₄⁻ only penetrates into the amorphous phase, thus rr- and rra-P3HT display similar IEs with B(Ph(CF₃)₂)₄⁻.



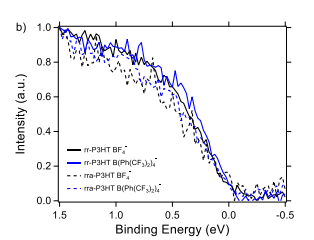


Figure 4. UPS spectra of rr-P3HT and rra-P3HT that are electrochemically doped with different anions in the electrolyte showing the secondary electron cut-off region (a) and the HOMO onset region (b).

The lower work function observed for rr-P3HT with BF₄⁻ is consistent with the fact that the film was electrochemically doped to a lower potential (ca. 0.34 V vs. Ag/Ag⁺) than the other films (0.5 to 0.6 V vs. Ag/Ag⁺). However, the work functions span a 0.8 eV range while the electrochemical doping potentials span a <0.3 V range. Considering the consistently higher work functions observed with B(Ph(CF₃)₂)₄⁻, we suspect that part of the differences may be explained by a higher doping concentration at the film surface with B(Ph(CF₃)₂)₄⁻ and B(Ph(CF₃)₂)₄⁻ accumulation at the surface. These UPS measurements and the variation in the

IEs of the doped polymers further highlight the important role of the anion structure in influencing the energetics and electronic structure of the electrochemically doped films.

3. Conclusion

The data presented support that larger anions such as B(Ph(CF₃)₂)₄⁻ have trouble penetrating into the crystalline regions found in rr-P3HT, while smaller anions such as BF₄⁻ can readily penetrate into the crystalline regions. This set of data has significant implications for determining the HOMO or LUMO energy by cyclic voltammetry or other electrochemical methods that rely on counterion penetration. For example, if a counterion that is unable to penetrate into the crystalline regions of the polymer is selected, then the extrapolated HOMO energy may reflect only the HOMO of the polymer in the amorphous phase. The counterion selected also impacts the nature of the polarons in the CP. In the case of rr-P3HT with B(Ph(CF₃)₂)₄⁻ the polaron absorbance displays distinct differences in comparison to rr-P3HT with BF₄⁻. These anion dependent polaron states are likely to significantly impact charge-carrier transport in doped CPs and a systematic understanding of how dopants and counterions impact electrical, optical, and thermoelectric properties will be essential to the continued developed of OSCs.

4. Experimental Section/Methods

Materials

Regioregular (91-94% regioregular, MW 50-70 kDa) and regiorandom (MW 70-90 kDa) poly(3-hexylthiophene-2,5-diyl) were purchased from Rieke Metals. Solutions of both polymers were prepared in anhydrous chlorobenzene (99.8%, extra dry) from Acros Organics. All electrolyte salts were purchased from Alfa Aesar except for lithium tetrafluoroborate which was purchased from Aldrich. All electrolyte solutions were prepared in anhydrous acetonitrile from VWR.

Film/Solution Preparation

Polymer solutions for both rr-P3HT and rra-P3HT were prepared at 15 mg/mL in chlorobenzene and stirred in a nitrogen atmosphere (<0.1 ppm H₂O and O₂) overnight before use. Polymer films were spun-cast onto glass substrates that were coated with indium tin oxide (ITO) at 1000 rpm with a 3 second ramp for 60 seconds. Films were then thermally annealed at 120 °C for 10 minutes to remove any extraneous solvent and promote crystallization. All electrolyte solutions were prepared at 10 mM concentration in acetonitrile and were stirred for several hours before use. All films were stored in the nitrogen filled glovebox after preparation.

Spectroelectrochemistry

Spectroelectrochemical measurements included the coupling of UV-Vis spectroscopy and cyclic voltammetry (CV). CV measurements were collected using a 1 cm pathlength quartz cuvette as the electrochemical cell. ITO coated glass substrates were used as the working electrode coupled with a Ag/Ag+ reference electrode (10 mM AgNO₃) and a platinum wire as the counter electrode. All electrodes were connected to the VersaStat4 electrochemical analyzer (Princeton Applied Research) and measurements were recorded using the VersaStudio software. UV-Vis measurements (350 nm to 1100 nm) were collected using a neutral density filter and a thermoelectric cooled fiber optic spectrometer (Ocean Optics). These measurements were performed outside of a glovebox in a Faraday cage with a continuous nitrogen purge. Measurements over an extended range (300 – 3300 nm) were conducted on an Agilent Technologies Cary 5000 UV–vis–NIR spectrophotometer. No significant differences in the overlapping regions of the spectra were observed between the rapid measurements recorded with the fiber optic spectrometer and the slower measurements recorded with the Cary 5000.

UPS

Sample for UPS were prepared on ITO coated glass using the same procedure as indicated above. The samples were electrochemically doped by increasing the voltage bias at

20 mV/s and removing the film from solution when it reached the first oxidation peak potential. Films were rinsed with acetonitrile, dried, and transferred into the ultra-high vacuum system. UPS measurements were performed using a PHI 5600 UHV system coupled with a hemispherical electron energy analyzer (28 cm diameter) and a multichannel detector. The photon source was an Excitech H Lyman-α lamp (E-Lux 121, 10.2 eV emission) with a 90° (E-Lux EEM Optical Module) and a dry oxygen purge through the beam path held between 7-10 Torr. A negative 5 V bias was applied to the samples during the measurements.

Supporting Information

Supporting Information is available from the Wiley Online Library or from the author.

Acknowledgements

We gratefully acknowledge support from the National Science Foundation (DMR-1905734).

Received: ((will be filled in by the editorial staff))
Revised: ((will be filled in by the editorial staff))
Published online: ((will be filled in by the editorial staff))

References

- 1. Boyle, C. J., Upadhyaya, M., Wang, P., Renna, L. A., Lu-Díaz, M., Pyo Jeong, S., Hight-Huf, N., Korugic-Karasz, L., Barnes, M. D., Aksamija, Z., Venkataraman, D. *Nat. Commun.*, 2019, **10**, 1–10.
- Ito, H., Mada, H., Watanabe, K., Tanaka, H., Takenobu, T. *Commun. Phys.*, 2021, 4, 1-9.
- 3. Lin, X., Wegner, B., Lee, K. M., Fusella, M. A., Zhang, F., Moudgil, K., Rand, B. P., Barlow, S., Marder, S. R., Koch, N., Kahn, A. *Nat. Mater.*, 2017, **16**, 1209–1215.
- 4. Pfeiffer, M., Beyer, A., Plönnigs, B., Nollau, A., Fritz, T., Leo, K., Schlettwein, D., Hiller, S., Wöhrle, D. *Sol. Energy Mater. Sol. Cells*, 2000, **63**, 83–99.
- 5. Lüssem, B., Riede, M., Leo, K. *Phys. status solidi*, 2013, **210**, 9–43.
- 6. Lin, Y., Firdaus, Y., Nugraha, M. I., Liu, F., Karuthedath, S., Emwas, A.-H., Zhang,

- W., Seitkhan, A., Neophytou, M., Faber, H., Yengel, E., McCulloch, I., Tsetseris, L., Laquai, F., Anthopoulos, T. D. *Adv. Sci.*, 2020, **7**, 1903419.
- 7. Khodagholy, D., Rivnay, J., Sessolo, M., Gurfinkel, M., Leleux, P., Jimison, L. H., Stavrinidou, E., Herve, T., Sanaur, S., Owens, R. M., Malliaras, G. G. *Nat. Commun.*, 2013, **4**, 2133.
- 8. Rivnay, J., Inal, S., Salleo, A., Owens, R. M., Berggren, M., Malliaras, G. G. *Nat. Rev. Mater.* 2018 32, 2018, **3**, 1–14.
- 9. Flagg, L. Q. Q., Giridharagopal, R., Guo, J., Ginger, D. S. *Chem. Mater.*, 2018, **30**, 5380–5389.
- 10. Guardado, J. O., Salleo, A. Adv. Funct. Mater., 2017, 27, 1701791.
- Harrelson, T. F., Cheng, Y. Q., Li, J., Jacobs, I. E., Ramirez-Cuesta, A. J., Faller, R.,
 Moulé, A. J. *Macromolecules*, 2017, 50, 2424–2435.
- Yang, C. Y., Ding, Y. F., Huang, D., Wang, J., Yao, Z. F., Huang, C. X., Lu, Y., Un,
 H. I., Zhuang, F. D., Dou, J. H., Di, C. an, Zhu, D., Wang, J. Y., Lei, T., Pei, J. Nat.
 Commun., 2020, 11, 1–10.
- Aubry, T. J., Winchell, K. J., Salamat, C. Z., Basile, V. M., Lindemuth, J. R., Stauber,
 J. M., Axtell, J. C., Kubena, R. M., Phan, M. D., Bird, M. J., Spokoyny, A. M., Tolbert,
 S. H., Schwartz, B. J. Adv. Funct. Mater., 2020, 30, 2001800.
- Cendra, C., Giovannitti, A., Savva, A., Venkatraman, V., McCulloch, I., Salleo, A.,
 Inal, S., Rivnay, J. Adv. Funct. Mater., 2019, 29, 1807034.
- Salzmann, I., Heimel, G., Oehzelt, M., Winkler, S., Koch, N. Acc. Chem. Res., 2016,
 49, 370–378.
- Jacobs, I. E., Lin, Y., Huang, Y., Ren, X., Simatos, D., Chen, C., Tjhe, D., Statz, M.,
 Lai, L., Finn, P. A., Neal, W. G., D'Avino, G., Lemaur, V., Fratini, S., Beljonne, D.,
 Strzalka, J., Nielsen, C. B., Barlow, S., Marder, S. R., McCulloch, I., Sirringhaus, H.
 Adv. Mater., 2021, 2102988.

- Liang, Z., Zhang, Y., Souri, M., Luo, X., Boehm, A. M., Li, R., Zhang, Y., Wang, T.,
 Kim, D. Y., Mei, J., Marder, S. R., Graham, K. R. J. Mater. Chem. A, 2018, 6, 16495–
 16505.
- 18. Untilova, V., Biskup, T., Biniek, L., Vijayakumar, V., Brinkmann, M. *Macromolecules*, 2020, **53**, 2441–2453.
- Un, H. I., Gregory, S. A., Mohapatra, S. K., Xiong, M., Longhi, E., Lu, Y., Rigin, S.,
 Jhulki, S., Yang, C. Y., Timofeeva, T. V., Wang, J. Y., Yee, S. K., Barlow, S., Marder,
 S. R., Pei, J. Adv. Energy Mater., 2019, 9, 1–10.
- 20. Liu, Z., Hu, Y., Li, P., Wen, J., He, J., Gao, X. J. Mater. Chem. C, 2020, 8, 10859–10867.
- Lu, G., Blakesley, J., Himmelberger, S., Pingel, P., Frisch, J., Lieberwirth, I.,
 Salzmann, I., Oehzelt, M., Di Pietro, R., Salleo, A., Koch, N., Neher, D. *Nat. Commun.*, 2013, 4, 1–8.
- 22. Marqués, P. S., Londi, G., Yurash, B., Nguyen, T. Q., Barlow, S., Marder, S. R., Beljonne, D. *Chem. Sci.*, 2021, **12**, 7012–7022.
- 23. Jacobs, I. E., Moulé, A. J. Adv. Mater., 2017, 29, 1703063.
- Jhulki, S., Un, H. I., Ding, Y. F., Risko, C., Mohapatra, S. K., Pei, J., Barlow, S.,
 Marder, S. R. *Chem*, 2021, 7, 1050–1065.
- 25. Zeng, Y., Zheng, W., Guo, Y., Han, G., Yi, Y. J. Mater. Chem. A, 2020, 8, 8323–8328.
- 26. Yao, W., Shen, L., Liu, P., Liu, C., Xu, J., Jiang, Q., Liu, G., Nie, G., Jiang, F. *Mater. Chem. Front.*, 2020, **4**, 597–604.
- Murrey, T. L., Riley, M. A., Gonel, G., Antonio, D. D., Filardi, L., Shevchenko, N.,
 Mascal, M., Moulé, A. J. *J. Phys. Chem. Lett.*, 2021, 12, 1284–1289.
- 28. Neusser, D., Malacrida, C., Kern, M., Gross, Y. M., Van Slageren, J., Ludwigs, S. *Chem. Mater.*, 2020, **32**, 6003-6013.
- 29. Baker, D. V., Bao, C., Kim, W. S. ACS Appl. Electron. Mater., 2021, 3, 2423–2433.

- 30. Friedlein, J. T., McLeod, R. R., Rivnay, J. Org. Electron., 2018, **63**, 398–414.
- 31. Djurovich, P. I., Mayo, E. I., Forrest, S. R., Thompson, M. E. *Org. Electron.*, 2009, **10**, 515–520.
- 32. Janietz, S., Bradley, D. D. C., Grell, M., Giebeler, C., Inbasekaran, M., Woo, E. P. *Appl. Phys. Lett.*, 1998, **73**, 2453.
- 33. Sworakowski, J., Janus, K. *Org. Electron.*, 2017, **48**, 46–52.
- 34. Sweetnam, S., Graham, K. R., Ngongang Ndjawa, G. O., Heumüller, T., Bartelt, J. A., Burke, T. M., Li, W., You, W., Amassian, A., McGehee, M. D. *J. Am. Chem. Soc.*, 2014, **136**, 14078–88.
- 35. Graham, K. R., Ndjawa, G. O. N., Conron, S. M., Munir, R., Vandewal, K., Chen, J. J., Sweetnam, S., Thompson, M. E., Salleo, A., McGehee, M. D., Amassian, A. *Adv. Energy Mater.*, 2016, **6**, 1-9.
- 36. Ibrahim, M. A., Lee, B.-G., Park, N.-G., Pugh, J. R., Eberl, D. D., Frank, A. J. *Synth. Met.*, 1999, **105**, 35–42.
- 37. Schwarze, M., Schellhammer, K. S., Ortstein, K., Benduhn, J., Gaul, C., Hinderhofer, A., Perdigón Toro, L., Scholz, R., Kublitski, J., Roland, S., Lau, M., Poelking, C., Andrienko, D., Cuniberti, G., Schreiber, F., Neher, D., Vandewal, K., Ortmann, F., Leo, K. *Nat. Commun.* 2019, 10, 1–9.
- 38. Acevedo-Peña, P., Baray-Calderón, A., Hu, H., González, I., Ugalde-Saldivar, V. M. *J. Solid State Electrochem.*, 2017, **21**, 2407–2414.
- 39. Al-Ibrahim, M., Roth, H. K., Schrödner, M., Konkin, A., Zhokhavets, U., Gobsch, G., Scharff, P., Sensfuss, S. *Org. Electron.*, 2005, **6**, 65–77.
- 40. Admassie, S., Inganäs, O., Mammo, W., Perzon, E., Andersson, M. R. *Synth. Met.*, 2006, **156**, 614–623.
- 41. Gayton, J. N., Autry, S., Fortenberry, R. C., Hammer, N. I., Delcamp, J. H. 2018, 23, 3051.

- 42. Valle, J. C. del, Blanco, F. G., Catalán, J. J. Phys. Chem. B, 2015, 119, 4683–4692.
- 43. Shaheen, S. A., Yang, M., Chen, B., Schlenoff, J. B. *Chem. Mater.*, 2020, **32**, 5994–6002.
- Flagg, L. Q., Bischak, C. G., Quezada, R. J., Onorato, J. W., Luscombe, C. K., Ginger,
 D. S. ACS Mater. Lett., 2020, 2, 254–260.
- 45. Giridharagopal, R., Flagg, L. Q., Harrison, J. S., Ziffer, M. E., Onorato, J., Luscombe,
 C. K., Ginger, D. S. *Nat. Mater.* 2017 167, 2017, 16, 737–742.
- 46. Liang, Z., Choi, H. H., Luo, X., Liu, T., Abtahi, A., Ramasamy, U. S., Hitron, J. A., Baustert, K. N., Hempel, J. L., Boehm, A. M., Ansary, A., Strachan, D. R., Mei, J., Risko, C., Podzorov, V., Graham, K. R. *Nat. Mater.*, 2021, **20**, 518–524.

Chemical and electrochemical doping of π -conjugated polymers are essential for many applications of organic semiconductors. In both chemical and electrochemical doping the ionized dopant or counterion can significantly impact the optical, electronic, and thermoelectric properties of the π -conjugated polymer. In this work we show how anions of varying size influence the oxidation potential, polaron absorbance, and ionization energy of both regioregular and regiorandom poly(3-hexylthiophene).

Kyle N. Baustert, Ashkan Abtahi, Ahmed Ayyash, Kenneth R. Graham*

Impact of the anion on electrochemically doped regionegular and regionandom poly(3-hexylthiophene)

ToC figure

